Spin reorientation and interplanar interactions of the two-dimensional triangular-lattice Heisenberg antiferromagnets *h*-(Lu,Y)MnO_3 and *h*-(Lu,Sc)FeO_3

S. Yano,[1] Junjie Yang,[2] Kazuki Iida,[3] Chin-Wei Wang,[1] Andrew G. Manning,[4] Daichi Ueta,[5] and Shinichi Itoh[5]

[1]*National Synchrotron Radiation Research Center, Hsinchu 30077, Taiwan*

[2]*Department of Physics, New Jersey Institute of Technology, Newark, New Jersey 07102, USA*

[3]*Neutron Science and Technology Center, Comprehensive Research Organization for Science and Society (CROSS), Tokai 319-1106, Ibaraki, Japan*

[4]*Australian Nuclear Science and Technology Organisation, Lucas Heights, NSW 2234, Australia*

[5]*Neutron Science Division, Institute of Materials Structure Science, High Energy Accelerator Research Organization, Tsukuba, Ibaraki 305-0801, Japan*

(Received 22 April 2024; revised 29 August 2024; accepted 10 October 2024; published 31 October 2024)

This study explored the magnetic properties and dynamics of two, two-dimensional (2D) triangular-lattice Heisenberg antiferromagnets (2D-TLHAF), *h*-(Lu,Y)MnO_3 and *h*-(Lu,Sc)FeO_3, through neutron powder diffraction, single-crystal neutron scattering, and polarized neutron-scattering experiments. We identified that the magnetic structures of both materials are described by two irreducible representations Γ_1 ($P6_3cm$) and Γ_2 ($P6_3c'm'$) for *h*-$Lu_{0.47}Sc_{0.53}FeO_3$, Γ_3 ($P6'_3cm'$), and Γ_4 ($P6'_3c'm$) for *h*-$Lu_{0.3}Y_{0.7}MnO_3$. Polarized neutron scattering has shown that accurately describing the magnetic structures of a 2D triangular-lattice Heisenberg antiferromagnet (2D-TLHAF) requires the use of two irreducible representations, rather than relying on the assumption that the system undergoes spin reorientation when using only one irreducible representation. We then investigated the spin-wave dispersion of both materials on the basis of these magnetic structures. The branch in the lowest energy of the spin wave of *h*-$Lu_{0.47}Sc_{0.53}FeO_3$ showed a flat dispersion along the *c* axis, while $Lu_{0.3}Y_{0.7}MnO_3$ displayed a distinct dispersion along the *c* axis, suggesting the presence of interplanar interactions in the latter. We discuss the potential causes of spin reorientation and multiferroicity in the triangular antiferromagnetic on the basis of the parameters determined.

DOI: 10.1103/PhysRevB.110.134444

I. INTRODUCTION

Spin reorientation is quite common among magnetic materials such as $\alpha - Fe_2O_3$ [1], Y-type hexa-ferrite $Ba_2Co_2Fe_{12}O_{22}$ [2], Fe_3BO_6 [3], MnP [4], Fe_7Se_8 [5], hexagonal *h*-*R*MnO_3 [6], hexagonal *h*-*R*FeO_3 [7,8], orthoferrites *o*-*R*FeO_3 [9], and orthochromites *o*-*R*CrO_3, where R = Sc, Y, or rare-earth metals [9]. This phenomena can occur for a variety of reasons. Among them, *h*-*R*MnO_3 and *h*-*R*FeO_3 are two-dimensional triangular-lattice Heisenberg antiferromagnets (2D-TLHAF) that are among the simplest playgrounds for geometrically frustrated antiferromagnetism, where low dimensionality and competing magnetic interactions often create interesting physics. Recent examples of such 2D-TLHAFs include (Y, Lu)MnO_3 [10], $LiCrO_2$ [11], $CuCrO_2$ [12], and (Lu, Sc)FeO_3 [7].

One of these hexagonal manganites, *h*-*R*MnO_3 [13], has been well studied and labeled type-I multiferroic materials. The crystal structure symmetry of *h*-*R*MnO_3 has been reported to be noncentrosymmetric $P6_3cm$, which has six possible representations: Γ_1 ($P6_3cm$), Γ_2 ($P6_3c'm'$), Γ_3 ($P6'_3cm'$), Γ_4 ($P6'_3c'm$), Γ_5 ($P6_3$), and Γ_6 ($P6'_3$) with a magnetic propagation vector k = (0,0,0). Among them, Γ_{1-4} are representations of one dimension and Γ_{5-6} are representations of two dimensions [14,15]. The magnetic structures of the *R*MnO_3 system have been characterized using Γ_1, Γ_2, Γ_3, and Γ_4, with a few variations shown in Fig. 1(b). For example, well-investigated compounds are $HoMnO_3$ and $YMnO_3$ that have the $P6_3cm$ symmetry.

The neutron polarimetry experiment with $HoMnO_3$, which provides evidence for the spin reorientation transition of Γ_4 to Γ_1 [14], is inconclusive due to Ho ordering [16]. However, it was concluded that Γ_3 was close to the correct ground state of $YMnO_3$, where the spins were rotated approximately 11 degrees from the Γ_3 state. The result shows that it is difficult to reliably determine the magnetic structure of this system even by a neutron polarimetry experiment.

One of the interesting physical effects observed in this system is the so-called trimerization, as shown in Fig. 1(a). The atomic position of Mn is placed close to ($x_{Mn} = 1/3$, 0 0) in the paramagnetic phase, making it an almost ideal triangular arrangement of the Mn atoms. Their position shifts away from the ideal value of $x_{Mn} = 1/3$ when the system enters the magnetically ordered state, as shown by the temperature dependence of the atomic position of Mn. Lee *et al*. reported [17] that $x_{Mn} = 0.3330(17)$ at 300 K at $x_{Mn} = 0.3423(13)$ at 10 K for $YMnO_3$, while a slightly smaller change was observed for $LuMnO_3$, but with the opposite sign. Magnetoelastic coupling causes trimerization, and this study claims that this is the primary origin of the multiferroic properties.

In addition to this, the value $x_{Mn} = 1/3$ is a critical threshold that determines the sign of effective interplanar exchange

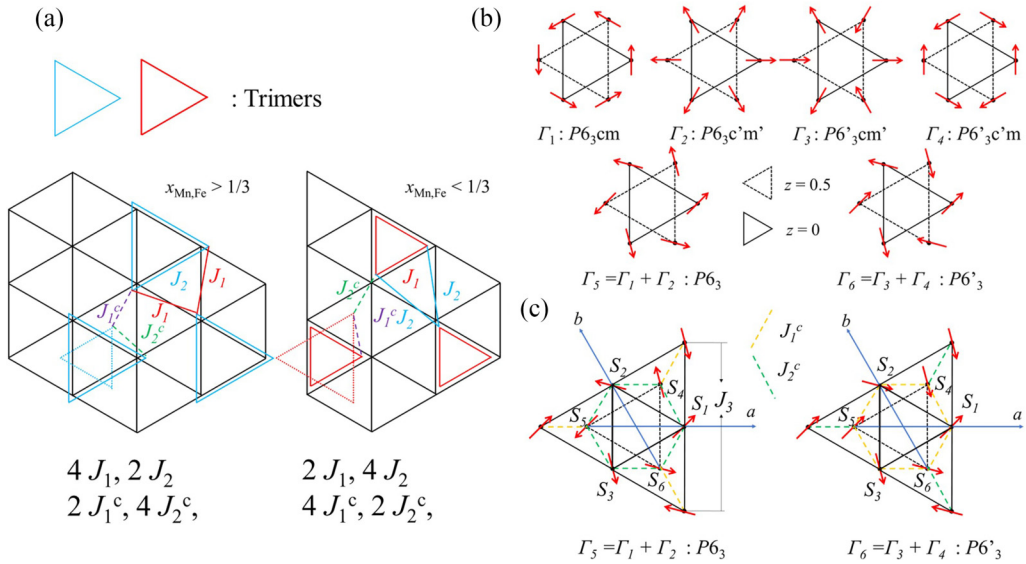

FIG. 1. (a) Triangular lattice formed by Mn atoms, with intraplanar exchange interactions (J_1 and J_2) and interplanar exchange interactions (J_1^c and J_2^c). The triangular lattice can be a perfect triangular when $x_{Mn} = 1/3$, where $J_1 = J_2$ and $J_1^c = J_2^c$. (b) Six irreducible representations under $P6_3cm$ symmetry, where Γ_1 to Γ_4 are irreducible one-dimensional representations, while Γ_5 and Γ_6 are irreducible two-dimensional representations. (c) The interactions between planes using examples of $\Gamma_5(P6_3)$ and $\Gamma_6(P6'_3)$.

interaction J_{z1}–J_{z2} [6] (we call them J_1^c and J_2^c), which sets the direction of the coupling within the Mn triangular plane. For instance, $HoMnO_3$ undergoes a transition from Γ_4 to Γ_1 at $x_{Mn} = 1/3$ and the spin-wave curve along the $(1, 0, l)$ direction is altered [6]. These *h*-$RMnO_3$ systems such as $HoMnO_3$ [14] and $ScMnO_3$ [18] display spin reorientation, while others such as $ErMnO_3$, $YbMnO_3$, $LuMnO_3$, and $YMnO_3$ do not because they do not cross the threshold. This is a significant discovery that contributes to a better understanding of spin reorientation in this system.

Many analyses of spin dynamics have been performed using inelastic neutron-scattering techniques on *h*-$RMnO_3$ [6,10,13,19–25]. The spin Hamiltonian can be described in J_1^c and J_2^c as interplanar exchange parameters. J_1 and J_2 are exchanges in the plane. Previous neutron-scattering experiments revealed a displacement in the atomic position of Mn from $(x_{Mn} = 1/3,\ 0,\ 0)$ [17], known as Mn trimerization, which leads to the presence of two distinct exchange parameters J_1 and J_2. The transition does not eliminate the rotational variance within the Mn plane but does impact the interactions between planes. D_1 and D_2 represent the easy-plane and in-plane easy-axis anisotropies [19], respectively. As shown above, the atomic position of $(x_{Mn} = 1/3, 0, 0)$ is a key parameter here. The first reason is that $x_{Mn} \neq 1/3$ creates two different exchange paths J_1 and J_2, and the second is that $x_{Mn} = 1/3$ is a critical position to determine the sign of effective exchange between planes $J_1^c - J_2^c$.

On the other hand, the hexagonal rare-earth ferrite *h*-$RFeO_3$ (R = Lu, Sc, Yb) family whose symmetry is also $P6_3cm$ represents another unique class of multiferroics exhibiting weak ferromagnetism, and a strong coupling between magnetism and structural trimerization is predicted as for *h*-$RMnO_3$. However, the hexagonal phase is rare, as only a few hexagonal phases of *h*-$RFeO_3$ have been reported, notably, $Yb_{0.42}Sc_{0.58}FeO_3$ [26] and $Lu_{0.50}Sc_{0.50}FeO_3$[27,28]. Interestingly, these *h*-$RFeO_3$ all show spin reorientation. The full range of spin dynamics in a bulk single crystal of *h*-$(Lu_{0.60}Sc_{0.40})FeO_3$ has been measured via time-of-flight inelastic neutron scattering, where the nearest-neighbor exchange coupling value was found to be $J = 4.0$ (2) meV from the linear spin-wave theory [29]. The experimentally measured parameters are compared with those obtained by density functional theory (DFT) calculations [26], which predicted that the exchange coupling constant for *h*-$LuFeO_3$ would be $J = 6.31$ meV in the plane. The spin dynamics of the *h*-(Lu, Sc)FeO_3 shows no spin-wave dispersion in the out-of-plane direction [29].

This study examines the phenomena of spin reorientation, multiferroicity, and spin-wave dispersion in two 2D-TLHAF compounds: manganese oxide Mn^{3+} ($S = 2$) and ferrites Fe^{3+} ($S = 5/2$). Our focus is on two compounds of 2D-TLHAFs, $Lu_{0.3}Y_{0.7}MnO_3$ and $Lu_{0.47}Sc_{0.53}FeO_3$, using neutron diffraction, magnetization, neutron-inelastic scattering, and polarized neutron-scattering techniques. Powder neutron diffraction was first used to uniquely determine the magnetic structures by using two irreducible representations. Polarized neutron scattering was then used to validate the magnetic structures determined, followed by inelastic neutron scattering to obtain the exchange parameters based on the refined structural parameters. We found obvious interplanar interactions in $Lu_{0.3}Y_{0.7}MnO_3$, while none were seen for $Lu_{0.47}Sc_{0.53}FeO_3$.

A. Experiment

Polycrystalline samples of $Lu_{0.47}Sc_{0.53}FeO_3$ were prepared both by solid-state reaction and pulverized from a single-crystal sample, denoted powder and polycrystalline samples, respectively. Single crystals of $Lu_{0.3}Y_{0.7}MnO_3$ and $Lu_{0.47}Sc_{0.53}FeO_3$ were prepared using the floating zone method. The weights of the sample were 4.0 and 2.7 grams.

Neutron powder diffraction was studied on the high-resolution powder diffractometer Echidna [30] installed at the Opal research reactor at the Australian Center for Neutron Scattering (ACNS) at the Australian Nuclear Science and Technology (ANSTO). The incident neutron wavelength of 2.4395 Å was selected by the Ge (331) reflection at a takeoff angle of 140 degrees. The sample was loaded into a 9-mm-diameter vanadium can and cooled with using a top-loading closed-cycle refrigerator.

Neutron-inelastic-scattering data was also collected in Sika [31,32] at ACNS in ANSTO and the high-resolution chopper spectrometer (HRC) [33,34] at the Japan Proton Accelerator Research Complex (J-PARC). Single-crystal samples were aligned in the (*h*0*l*) and (*hk*0) for the experiments in Sika to complete the data shown in this paper. The sample was aligned in the *ab* plane, and the incident energy $E_i = 35$ meV was chosen to obtain a complete dispersion pattern of $Lu_{0.3}Y_{0.7}MnO_3$ on HRC. The spin dynamics of $Lu_{0.47}Sc_{0.53}FeO_3$ were collected with Sika, and the final energy was fixed at $E_f = 5$ meV with collimations open-open-60′-60′. A Be filter was in place on the scattered side to cut off the higher-order wavelengths.

For the polarized neutron-scattering experiment, the ^{3}He polarization system was installed on Sika at ACNS in ANSTO. The fully automated arms of the spin polarizer and analyzer used the Pastis coil to control the spin direction [35,36]. The experiment allows us to collect diagonal components of polarization matrices shown later in the text.

B. Discussion about the magnetic structure of 2D-TLHAF in general

Under the $P6_3cm$ symmetry with a propagation vector $k = (0,0,0)$, Γ_{1-4} are one-dimensional representations and Γ_{5-6} are two-dimensional representations [14,15]. These Γ_1, Γ_2, Γ_3, and Γ_4 representations have frequently been used to describe the magnetic structures of *h*-*R*MnO_3 or *h*-*R*FeO_3. In prior research, the investigation of $Lu_{0.3}Y_{0.7}MnO_3$ revealed a Néel temperature of $T_N = 80$ K, without any observed spin reorientation [37]. Conversely, $Lu_{0.5}Sc_{0.5}FeO_3$ exhibited transition temperatures of $T_N = 172(1)$ K and spin reorientation temperature $T_{SR} = 45(1)$ K [27].

It is known that Γ_1 and Γ_3 contribute to the magnetic Bragg peak intensity at (100) [8], and the calculated magnetic scattering intensities of Γ_2 and Γ_4 are zero at (100), so that if there is no (100) peak but the (101) peak is present, the magnetic structure is assumed to be Γ_2 or Γ_4. If one chooses to utilize a single irreducible representation for solving the magnetic structure, spin reorientation should occur such as (Γ_2 to Γ_1), (Γ_4 to Γ_2) and so on because of the (100) peak that appears or disappears at T_{SR}. Note that the (100) peak is very weak in the nuclear structure factor of a system with $P6_3cm$ symmetry, and it cannot be the result of trimerization [Fig. 1(a)].

C. Crystal and magnetic structures of (Lu,Sc)FeO_3

Using a powder neutron diffractometer, we have studied magnetic structures using both a powder sample and a polycrystalline sample of (Lu,Sc)FeO_3. The compositions of the samples were confirmed by Rietveld refinement, with the powder sample identified as $Lu_{0.60}Sc_{0.40}FeO_3$ and the polycrystalline sample as $Lu_{0.61}Sc_{0.39}FeO_3$.

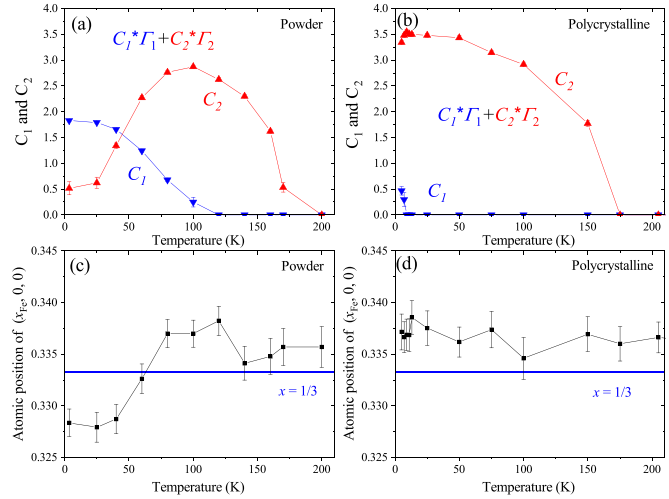

FIG. 2. The temperature dependence of magnetic structure of (Lu,Sc)FeO_3. Coefficients of two irreducible representations for the (a) powder sample and (b) pulverized single-crystal sample. Atomic position of the x_{Fe} at the (x_{Fe}, 0, 0) site for the (c) powder sample and (d) pulverized single-crystal sample.

The temperature dependence of the coefficients C_1 and C_2 for the overall magnetic structures of the form $C_1\Gamma_1 + C_2\Gamma_2$ is shown in Fig. 2, which highlights the difference between the powder and polycrystalline samples. For temperatures $T_N \sim 160 < T < T_{SR}$, the magnetic structure of $Lu_{0.60}Sc_{0.40}FeO_3$ can be described exclusively with Γ_2 with $C_1 = 0$. However, below T_{SR} the magnetic (100) Bragg peak appears, and both Γ_1 and Γ_2 were used to fit the magnetic structures. The transition temperature T_{SR} is higher for the powder compared to the polycrystalline samples made from pulverized single crystals, which is consistent with other studies on *h*-*R*FeO_3 [7,8,27]. Conversely, the low polycrystalline T_{SR} is consistent with the single-crystal sample of $Lu_{0.47}Sc_{0.53}FeO_3$, as shown in Fig. 3, where T_{SR} is clearly observed coincidentally with the appearance of the magnetic Bragg (100) peak at $T = 15.5$ (2) K. Thus, the spin reorientation temperature of the single crystal is similar to that of the polycrystalline sample, rather than the powder sample.

Figures 2(a) and 2(b) show temperature dependences of coefficients C_1 and C_2 of these magnetic structures $C_1\Gamma_1 + C_2\Gamma_2$ for the polycrystalline sample and the polycrystalline sample. In the powder sample, C_1 grew at 100 K, where C_2 decreases, while in the polycrystalline sample, the Γ_1 phase appears only below 10 K and Γ_2 dominates at most temperatures. The ferromagnetic component observed in magnetization suggests that the preferable model is $C_1\Gamma_1 + C_2\Gamma_2$ over $C_3\Gamma_3 + C_4\Gamma_4$ because only Γ_2 can have the ferromagnetic component, and Γ_1 is the only magnetic structure that can explain the powder diffraction pattern in combination with Γ_2 to accurately reproduce the diffraction pattern. The ferromagnetic component of Γ_2 is too weak to be determined from the neutron powder diffraction data. Because of that, it is difficult to determine the magnetic structure of this system by using polycrystalline samples and even single-crystal samples.

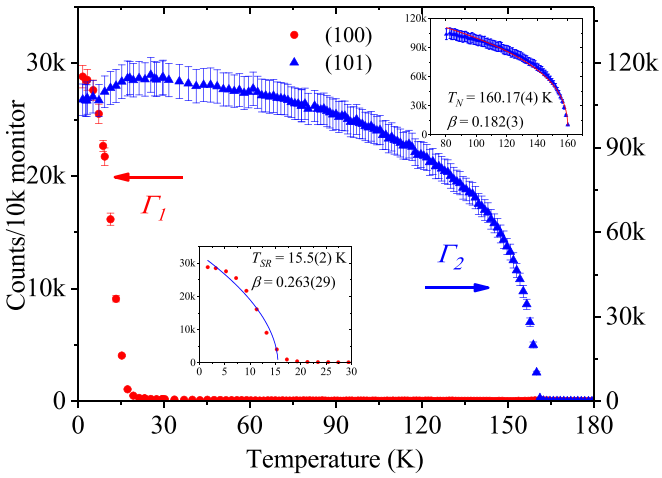

FIG. 3. Temperature dependence of the scattering intensities of the (100) and (101) magnetic Bragg peaks for the single-crystal sample of $Lu_{0.47}Sc_{0.53}FeO_3$, with insets highlighting the transition temperatures.

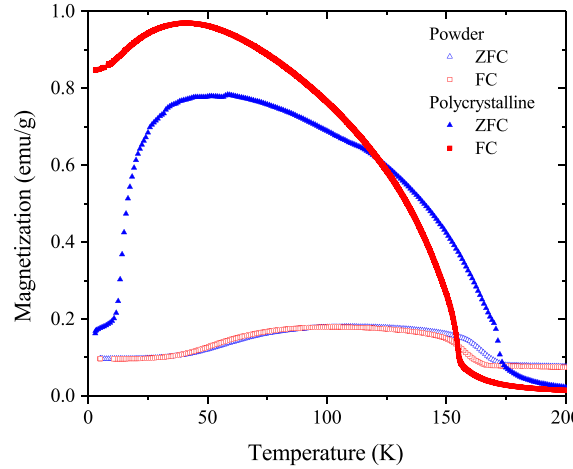

FIG. 4. Magnetization of powder sample $Lu_{0.60}Sc_{0.40}FeO_3$ and polycrystalline sample of $Lu_{0.61}Sc_{0.39}FeO_3$ measured at $H = 500$ Oe.

Interestingly, there are also differences in trimerization [17], as shown in Figs. 2(c) and 2(d). The powder sample shows trimerization below 70 K where $x_{Fe} < 1/3$, while no clear trimerization was observed in the polycrystalline sample. In previous studies of $Lu_{1-y}Y_yMnO_3$ [37], we found that the magnetic structure of $Lu_{0.3}Y_{0.7}MnO_3$ is described as a linear combination of Γ_3 and Γ_4 equivalent to Γ_6 ($P6'_3$). The atomic position of Mn remains $x_{Mn} = 1/3$, which is one of the key parameters for the reorientation of the spin of $RMnO_3$. So far, there has been no systematic study to see the difference between polycrystalline samples and powder samples of *h*-$RMnO_3$ or *h*-$RFeO_3$. The result indicates that this dedicated parameter can behave differently in different samples, as shown in Figs. 2 and 3. The polycrystalline sample shows $x_{Fe} \geqslant 1/3$ in the temperature range below 200 K. Because of that, we expect the interplanar interaction of the single crystal of $Lu_{0.47}Sc_{0.53}FeO_3$ [6].

The magnetic Bragg peak (100) appears at different temperatures in the single-crystal sample. Because the signal-to-noise ratio of the magnetic Bragg peaks is normally better for the single-crystal sample, the difference between two samples is interesting. Single-crystal and polycrystalline samples show a clear transition below 20 K. For the powder form of the samples, spin reorientation of $(Lu_{0.5}Sc_{0.5})FeO_3$ at $T_{SR} \sim 50$ K [27], $(Lu_{0.6}Sc_{0.4})FeO_3$ at $T_{SR} \sim 100$ K in this work, and $(Yb_{0.42}Sc_{0.5})FeO_3$ at $T_{SR} \sim 40$ K [8] has been reported. The quality of the sample could influence the spin reorientation.

The transition temperatures for the single-crystal sample were found to be $T_N = 160.17(4)$ K and $T_{SR} = 15.5(2)$ K with critical exponents $\beta = 0.182(3)$ and 0.263(29) by fitting the magnetic (101) and (100) peak intensities, respectively, using $I(T) = A(1 - T/T_{SR,N})^{2\beta}$, where A is for normalization. At T_{SR}, there is a slight drop in intensity at (101) while the (100) reflection emerges. Like the β found for $YMnO_3$, β at T_N for $Lu_{0.47}Sc_{0.53}FeO_3$ do not correspond to any of the well-known universality classes. This is because the critical region is greatly extended by magnetic frustration [38]. The frustration is released at T_N so that β at T_{SR} is close to β for a typical 2D XY antiferromagnet whose theoretical value $\beta = 0.23$.

Figure 4 illustrates the magnetization measurements of the same powder and polycrystal samples as were investigated with neutron powder diffraction. The presence of ferromagnetism is associated with the Γ_2 phase. Interestingly, the ferromagnetic aspect of the polycrystalline sample persists at a lower temperature compared to the powder sample, supporting the existence of a weak ferromagnetic phase from the Γ_2 magnetic structure as seen in the powder neutron diffraction data.

D. Polarized neutron scattering of the single crystal of $Lu_{0.47}Sc_{0.53}FeO_3$

We studied magnetic peaks in the ($h0l$) plane to distinguish the magnetic structure using polarized neutron scattering for the single-crystal sample of $Lu_{0.47}Sc_{0.53}FeO_3$. Precise magnetic structure determination is important to determine the spin Hamiltonian of the 2D-TLHAF structure. Since using $C_1\Gamma_1 + C_2\Gamma_2 = \Gamma_5$ and $C_3\Gamma_3 + C_4\Gamma_4 = \Gamma_6$ gives us the same structure factor and we cannot easily see the weak ferromagnetic component with unpolarized neutron diffraction, determining the true magnetic structure is challenging. This remains the case even if we use single-crystal samples with polarized neutron scattering, as mentioned in Brown and Chatterji's work [16]. Regarding $YMnO_3$, the scattering of polarized neutrons supports the conclusion that the magnetic structure is Γ_3 but was still inconclusive. However, in the case of $(Lu,Sc)FeO_3$, by conducting a polarized neutron-scattering experiment we can effectively identify the magnetic structure of $Lu_{0.47}Sc_{0.53}FeO_3$ by specifically examining its ferromagnetic component.

Here, we show the two peaks of the magnetic peaks (101) and (103) from the single-crystal sample of $Lu_{0.47}Sc_{0.53}FeO_3$ in Fig. 5 and Table I. The nonmagnetic peak (004) at $T = 300$ K was used for the calibrations for the neutron spin filter system. The peak shows about 90 percent of the neutron scattering as a non-spin-flip (NSF) process, while the rest of the neutrons scatter as a SF process, which demonstrates the performance of the spin filters. Here, Bragg peaks ($h0l$)

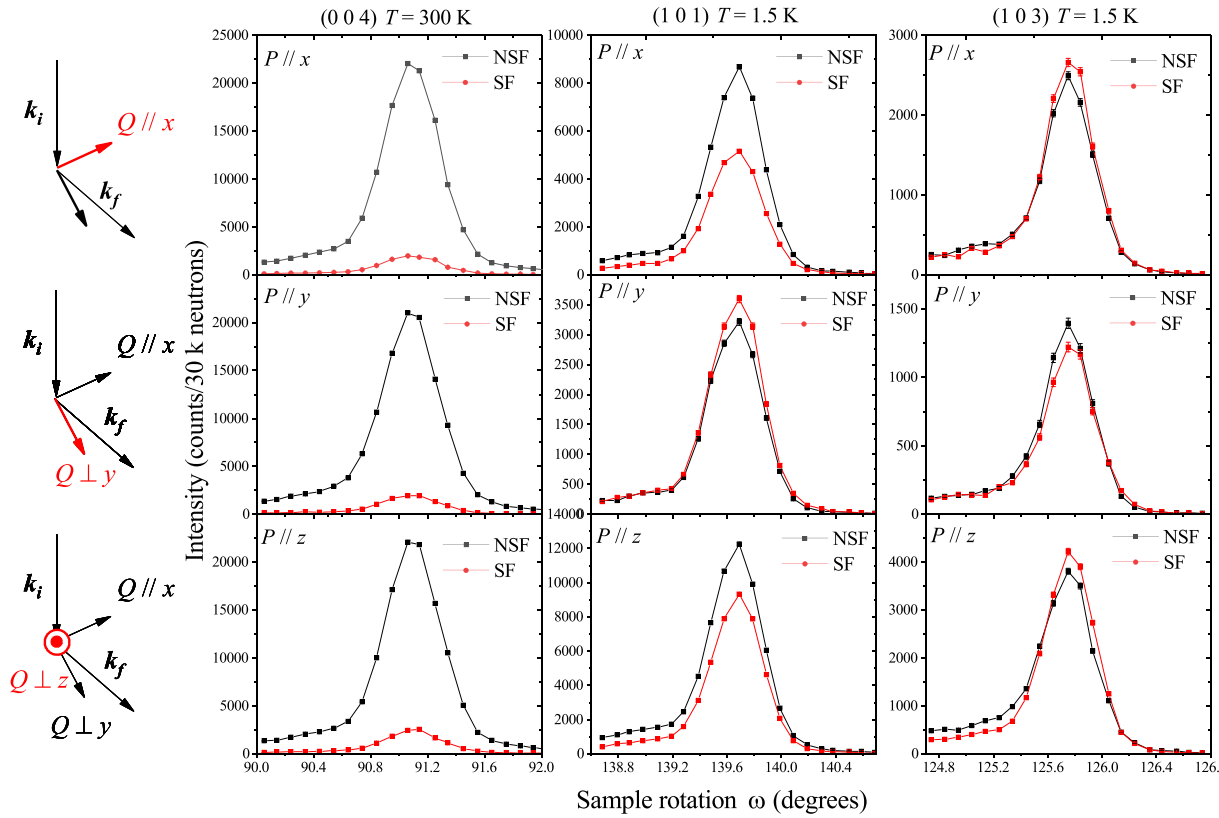

FIG. 5. The representative polarization dependence of Bragg peaks. The purely nuclear Bragg peak (004) at $T = 300$ K is used for calibration. The (101) and (103) Bragg peaks are mainly due to magnetic scattering. The k_i, k_f, and Q are incident neutron wave vector, scattered neutron wave vector, and scattering wave vector, respectively.

with odd l have zero nuclear structure factors due to the systematic absence imposed by the glide plane c of $P6_3cm$. These peak intensities are purely magnetic, and given that we are sensitive to the component of magnetism perpendicular to the scattering plane, they will reveal the orientation of the magnetic structure.

We define the x, y, z axes as Q(h 0 l) //x, Q(h 0 l) $\perp$ y in the scattering plane, and Q(h 0 l) $\perp$ z out of the scattering plane, where magnetism in the y direction will be seen in the x and z directions. The measurements which compare the relative scattering amplitude for neutrons polarized in each of these directions are summarized in Table I. P_{xx} and P_{zz} change from plus for (101) to minus (103) at 1.5 and 30 K. The portion of spin-flip-polarized neutrons increases while increasing l, which means that there is a magnetic component along the c axis. The magnetic component along the y flips more neutrons, because the reduction in the ferromagnetic component along the c axis is projected by increasing l. The

TABLE I. Diagonal elements of the polarization matrices of (101) and (103) reflections from $Lu_{0.47}Sc_{0.53}FeO_3$.

$Lu_{0.47}Sc_{0.53}FeO_3$	$(101)_{T=1.5\,K}$	$(103)_{T=1.5\,K}$	$(101)_{T=30\,K}$	$(103)_{T=30\,K}$
P_{xx}	0.251(8)	–0.06(1)	0.155(9)	–0.06(2)
P_{yy}	–0.05(1)	0.07(2)	-0.05(1)	0.02(2)
P_{zz}	0.133(7)	–0.08(1)	0.079(7)	–0.12(1)

P_{yy} is slightly minus for the (101) peak and changes to plus for the (103) peaks in both $T = 1.5$ and 30 K, where the ferromagnetic component along the c axis projected on the plane decreases with increasing l, so it results in a reduction in the spin-flip process. The results support the fact that the ferromagnetic component c-component exists in both 1.5 and 30 K. Note that the only irreducible representation leading to the ferromagnetic component along the c axis is Γ_2 ($P6_3c'm'$), which will be discussed with Table II [39] in the Discussion section.

On the basis of all the information mentioned above, the magnetic structural analysis procedures are as follows. The result shows that the 1.5-K and 30-K phases have a weak ferromagnetic component along the c axis. In that case, to describe the magnetic structure of $Lu_{0.47}Sc_{0.53}FeO_3$, the irreducible representation of Γ_2 should be included in both 1.5 and 30 K. In addition to this, since the magnetic (100) peak is observed below T_{SR}, either Γ_1 or Γ_3 should be included. In that case, if Γ_2 were included, $\Gamma_5 = C_1\Gamma_1 + C_2\Gamma_2$ is the only model that can fit the powder neutron diffraction patterns of powder and polycrystal samples of (Lu,Sc)FeO_3. So we conclude that we need to use two irreducible representations to describe the magnetic structures of $Lu_{0.47}Sc_{0.53}FeO_3$.

On the other hand, we argue that $\Gamma_6 = C_3\Gamma_3 + C_4\Gamma_4$ for $Lu_{0.3}Y_{0.7}MnO_3$ and $\Gamma_5 = C_1\Gamma_1 + C_2\Gamma_2$ for $Lu_{0.47}Sc_{0.53}FeO_3$ is a better model to use considering the result of polarized neutron scattering. We summarize the characteristic of irreducible representations in Table II. In the case of $LuMnO_3$, $YMnO_3$,

TABLE II. Summary of magnetic properties of each irreducible representations of $P6_3cm$ [39].

$P6_3cm$	Γ_1 ($P6_3cm$)	Γ_2 ($P6_3c'm'$)	Γ_3 ($P6'_3cm'$)	Γ_4 ($P6'_3c'm$)
Moments out of the *ab* plane	No	Yes	No	Yes
Weak ferromagnetism along the *c* axis	No	Yes	No	No
Magnetic peak (100)	Yes	No	Yes	No
Magnetoelectric coupling	$P_xM_y - P_yM_x$	$P_xM_y + P_yM_x, P_zM_z$	No	No

and $Lu_{1-y}Y_yMnO_3$, there have not been any ferromagnetic moments reported so far using magnetization measurements, and thus we do not have positive evidence to determine that $\Gamma_6 = C_3\Gamma_3 + C_4\Gamma_4$ is the correct magnetic structure of $Lu_{1-y}Y_yMnO_3$. However, an antiferromagnetic moment along the *c* axis observed in $YMnO_3$ based on resonant x-ray diffraction [40] and the newly proposed magnetic structure does not contradict our model [39,41]. If we used Γ_4, only the magnetic structure that fits our neutron powder diffraction data is $\Gamma_6 = C_3\Gamma_3 + C_4\Gamma_4$. Also, the total energy of different magnetic configurations obtained by Hartree-Fock calculation for a low-energy model supports that the magnetic structure of $YMnO_3$ is Γ_3 and that of $LuMnO_3$ is Γ_4 [42].

The reason why spin reorientation is observed in the 2D-TLHAF is because the (100) peaks show up at certain temperatures. Only the magnetic structures Γ_1 and Γ_3 have a magnetic scattering intensity at the (100) peak, while the calculated magnetic scattering intensities for Γ_2 and Γ_4 are zero. If only one irreducible representation is used to solve the magnetic structure, spin reorientation should occur. As shown here, in the case of 2D-TLHAF, if we could use two irreducible representations to describe the magnetic structure, there might be no drastic magnetic structural change like spin reorientation, and the magnetic structure could change gradually while changing the temperatures of the system by changing the ratio of two irreducible representations.

It is also noted that the inhomogeneity of Sc, Y, or Lu is not an issue because additional peaks or Bragg peak separation from two or more different lattice parameters (such as $LuMnO_3$, $YMnO_3$, $LuFeO_3$, or $ScFeO_3$) were not observed in any of the powder neutron diffraction, polarized neutron-scattering, or inelastic neutron-scattering (the latter section) data sets. From instrumental Q and energy resolutions, these samples should be recognized as single-phase samples.

E. Analysis of spin waves in 2D-TLHAF in general

In the preceding sections we have outlined the process of determining the magnetic structures of the 2D-TLHAF system. We then conducted neutron-inelastic scattering experiments to ascertain the exchange parameters of this system. The spin Hamiltonian can be expressed as

$$H = \sum_{\langle i,j\rangle\text{intra}} J_n \mathbf{S}_i \cdot \mathbf{S}_j + \sum_{\langle i,j\rangle\text{inter}} J_n^c \mathbf{S}_i \cdot \mathbf{S}_j + H_{\text{aniso}}. \quad (1)$$

The intraplanar exchange parameters, J_1, J_2, and J_3, the spin Hamiltonian can be expressed in terms of the intratrimer interaction J_1, the intertrimer interaction J_2, and the third-nearest-neighbor interaction J_3, as well as the interplanar exchange parameters J_1^c and J_2^c as shown in Figs. 1(a) and 1(c). Fabréges *et al*. [6] noted that spin reorientation is largely dependent on the value of $J_1^c - J_2^c$. The anisotropic term in the Hamiltonian is

$$H_{\text{aniso}} = D_1 \sum_i \left(\mathbf{S}_i^z\right)^2 + D_2 \sum_i (\mathbf{S}_i \cdot \mathbf{n}_i)^2, \quad (2)$$

where D_1 and D_2 represent the easy-plane and in-plane easy-axis anisotropies [19]. The anisotropy D_2 is parallel to the spin directions, i.e., $\mathbf{n}_i = \langle \mathbf{S}_i \rangle / |\langle \mathbf{S}_i \rangle|$.

Oh *et al*. [10,13] improved the models by including a magnetoelastic coupling term to explain magnon decay in $LuMnO_3$, $Y_{0.5}Lu_{0.5}MnO_3$, and $YMnO_3$ [10], using $J_1 = J_2$ to explain the low-energy portion. They noticed that linear spin-wave theory was inadequate due to the downward curvature in the *AB* direction, the additional peak at around 19 meV in the *OB* direction, and an abnormally large J_1/J_2 ratio. The magnetoelastic coupling model of superexchange striction qualitatively reproduces the observation of the experiment on $YMnO_3$ [43]. Holm *et al.* combined Zeeman splitting with the information of magnon and phonon intensities in the case of $YMnO_3$ [22], where Γ_2 and Γ_4 are excluded. The other two ground states, Γ_1 and Γ_3, are generally compatible with the observations. In addition, their model could give these states, as Γ_1 and Γ_3 are not homometric in the inelastic channel, while the data are not of sufficient quality to uniquely distinguish the two states.

F. Spin-wave dispersion of $Lu_{0.3}Y_{0.7}MnO_3$

Some of the *h*-*R*MnO_3 systems show no spin reorientation, such as $ErMnO_3$, $YbMnO_3$, $LuMnO_3$, and $YMnO_3$. To investigate one of these 2D-TLHAFs, we chose the x_{Mn} controlled compound $Lu_{0.3}Y_{0.7}MnO_3$, because x_{Mn} is close to 1/3 and does not change below or above T_N, and Lu and Y are nonmagnetic atoms.

The magnetic structure of the material was found to be a combination of Γ_3 and Γ_4 based on previous reports [37], and no distinct spin reorientation was observed. The proportion of Γ_3 and Γ_4 varies with changes in temperature and the composition of Lu and Y. In the ground state, $YMnO_3$ and $LuMnO_3$ exhibit different magnetic structures Γ_3 and Γ_4. The total energies of various magnetic configurations were determined using Hartree-Fock calculations for the low-energy model. The discrepancy in the magnetic structures of $YMnO_3$ and $LuMnO_3$ can be attributed to the behavior of single-ion anisotropy, which corresponds to the distortion of the Mn triangles.

The spin-wave dispersion is shown for $Lu_{0.3}Y_{0.7}MnO_3$ in Fig. 6, and specifically along the l direction in Fig. 7. The parameters determined are $J_1 = 7.43(1)$ meV, $J_2 = 1.42(1)$ meV, $J_3 = 0.02(1)$ meV, $J_1^c = -0.012(1)$ meV, $J_2^c = 0$ (fixed), $D_1 = 0.244(1)$ meV, and $D_2 = -0.028(1)$ meV, as

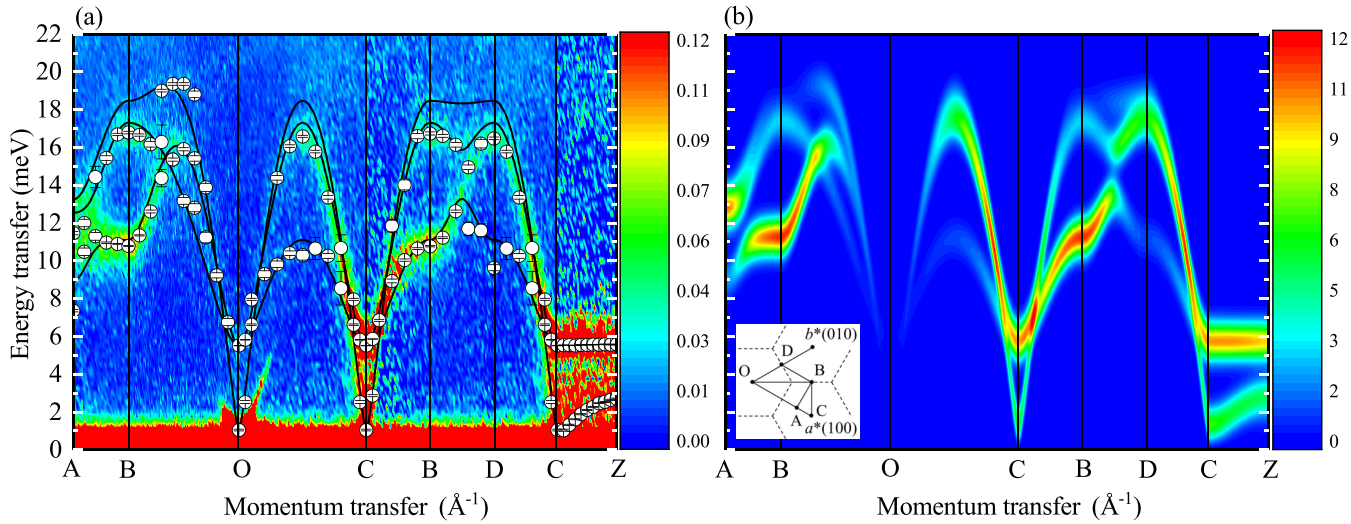

FIG. 6. (a) Spin-wave dispersion relation of the $Lu_{0.3}Y_{0.7}MnO_3$ obtained at HRC, J-PARC at 5 K. The dots are determined by the constant Q cut from the neutron-scattering data. The lines are obtained by fitting these dots using the least-squares method. (b) Calculation of the dynamical structure factor using linear spin-wave theory.

summarized in Table III. These parameters are determined by fitting the dispersion relations obtained by the experiment, as shown in Fig. 6(a). The calculation of spin waves based on the linear spin-wave theory in Fig. 6(b) by using these parameters matches the data in Fig. 6(a) well. Oh *et al.* claim that the DFT calculations show only a 10–20 percent difference between J_1 and J_2 [10,44].

The strong magnetoelastic coupling in RMnO$_3$ is evident from the drastic change in many physical properties at T_N supported by many measurements of physical properties such as, neutron diffraction [17] and inelastic neutron-scattering experiments [10,13]. We observed a similar excitation at an energy transfer of approximately 19 meV in the OB direction in Fig. 6(a). Oh *et al.* successfully model the branch by introducing magnetoelastic coupling and dimensionless exchange-striction parameters α [10]. In our scenario, the optimized parameters obtained via linear spin-wave theory are sufficient to describe this branch without incorporating magnetoelastic coupling, primarily by adjusting the ratio J_1/J_2. Incorporating magnetoelastic coupling as described in [10] was beyond the scope of our study.

As demonstrated in Fig. 7, the clear dispersion of Δ_1 shows that interactions exist along the l direction. With this information in mind, the exchange parameters determined using the full dispersion are $J_1^c - J_2^c = -0.012$ (1) meV in $Lu_{0.3}Y_{0.7}MnO_3$. To compare with another 2D-TLHAF, HoMnO$_3$ changes from $J_1^c - J_2^c = -0.0038(5)$ meV at $T = 45$ K $> T_{SR}$ to $J_1^c - J_2^c = 0.0018(5)$ meV at $T = 27$ K $< T_{SR}$. Therefore, the spin dispersion curvature along l and the sign of $J_1^c - J_2^c$ change and cause spin reorientations in HoMnO$_3$. The case of $Lu_{0.3}Y_{0.7}MnO_3$, similar to HoMnO$_3$ at 45 K and YbMnO$_3$ at 2 K, where the low-energy branch of the spin-wave dispersion trends upward along the $(10l)$ direction, is summarized in Table IV.

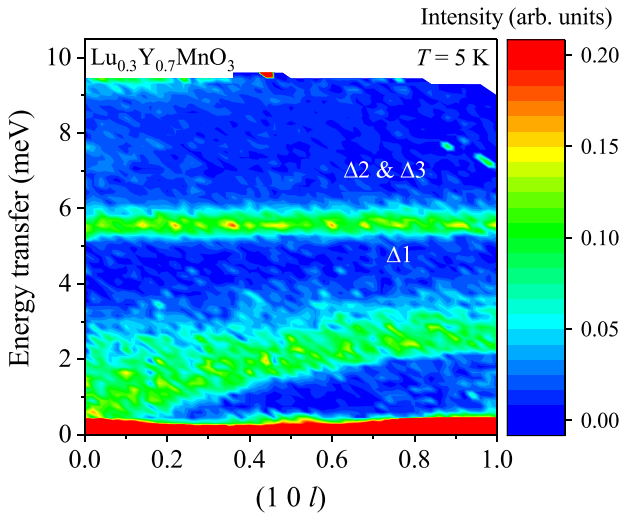

FIG. 7. Spin-wave dispersion relation along the l direction obtained at HRC, J-PARC at 5 K.

G. Spin-wave dispersion of $Lu_{0.47}Sc_{0.53}FeO_3$

The other type of h-RMnO$_3$ and h-RFeO$_3$ shows spin reorientation, such as HoMnO$_3$ (Γ_4 to Γ_1), ScMnO$_3$ (Γ_2 to Γ_3), $Yb_{0.5}Sc_{0.5}FeO_3$, and $Lu_{0.5}Sc_{0.5}FeO_3$ (Γ_2 to Γ_1). As demonstrated so far, h-$Lu_{0.47}Sc_{0.53}FeO_3$ shows a clear magnetic (100) peak below 15.5 K. The reported h-RFeO$_3$ systems are rare, but each exhibits spin reorientation. Here, we study the magnetic excitation of $Lu_{0.47}Sc_{0.53}FeO_3$ in two phases ($T = 1.5$ and 30 K) below and above $T_{SR} = 15.5$ K.

Figures 8 and 9 show the dispersion of the spin waves at 1.5 and 30 K. The dispersions at 1.5 and 30 K are almost identical except for the Bose factor. Unlike $Lu_{0.3}Y_{0.7}MnO_3$, there is no dispersive mode in the lower part of the spin-wave dispersion on $Lu_{0.47}Sc_{0.53}FeO_3$, even though a clear spin reorientation is observed. Other 2D-TLHAFs, such as HoMnO$_3$, show that the curvature of the spin-wave dispersion at low energy changes from upwards ($T = 45$ K and Γ_4) to downwards ($T = 27$ K and Γ_1). Such a clear transformation was not observed in

TABLE III. The determined exchange parameters of some of the 2D-THLA systems obtained in this work and other literature.

2D-TLHAFs	J_1	J_2	J_3	$J_1^c - J_2^c$ (Fixed)	D_1	D_2	
$YMnO_3$	3.4(2)	2.02(7)	–	0.014(2)	0.28	–0.0007(6)	[19]
$Lu_{0.3}Y_{0.7}MnO_3$	7.43(1)	1.42(1)	0.02(1)	–0.012(1)	0.244(1)	–0.028(1)	This work
	3.24(2)	2.70(1)	–	0	0.300(1)	–0.0013(1)	[37]
	2.65(5)	2.32(5)	–	–0.0012(4)	0.44(1)	0	[24]
$Lu_{0.5}Y_{0.5}MnO_3$	3	3	–	–	0.28	–0.02	[10]
$LuMnO_3$	4.09	1.54	–	–0.019(2)	0.44	0	[23]
$Lu_{0.6}Sc_{0.4}FeO_3$	4.0	4.0	–	–	0.17(1)	–0.05(1)	[29]

$Lu_{0.47}Sc_{0.53}FeO_3$ below and above the spin reorientation transition temperature.

The current findings suggest that the spin reorientations in these two $Lu_{0.3}Y_{0.7}MnO_3$ and $Lu_{0.47}Sc_{0.53}FeO_3$ are not as significant as previously reported in *h*-*R*MnO_3 and *h*-*R*FeO_3 systems. Spin reorientations can be understood as a reconfiguration of the magnetic structure by changing the ratios of C_1 and C_2 for Γ_1 and Γ_2. The presence of a weak ferromagnetic element along the z axis indicates the presence of a magnetic phase characterized by the irreducible representation of Γ_2. Magnetoelectric coupling is possible through Γ_1 and Γ_2, so even though the crystal and magnetic structures are similar to those of *h*-*R*MnO_3, the origin of the multiferroicity of *h*-*R*FeO_3 can be different from that of *h*-*R*MnO_3.

In the case of $Lu_{0.47}Sc_{0.53}FeO_3$, the dispersion along $(10l)$ is flat, indicating that the interactions between planes are very weak or have been canceled, leading to $J_1^c - J_2^c \sim 0$. The three branches that we observed $Lu_{0.3}Y_{0.7}MnO_3$ become two branches, as shown in Fig. 10. Leiner *et al.* obtained the full spin-wave dispersion of *h*-$Lu_{0.6}Sc_{0.4}FeO_3$ [29], with instrumental energy resolution being 2.5 meV FWHM for the elastic line at $E_i = 45$ meV [29]. To more precisely differentiate, we performed measurements using a cold triple-axis spectrometer Sika, achieving a higher energy resolution of approximately 0.15 meV in the elastic line with a fixed $E_f = 5$ meV. In addition, the gaps of Δ_1 and Δ_2 at (100) disappear at $T_N = 160$ K, indicating that these dispersions of $Lu_{0.47}Sc_{0.53}FeO_3$ are magnons. The disappearance of the flat dispersion at T_N was also observed in another measurement on the instrument HRC at J-PARC (not shown in this paper). So, they are not phonons or artificial excitations (spurions) due to different instrument configurations or sample environment.

By using the same spin Hamiltonian, the analytical forms of the spin-wave gap for *h*-(Lu, Y)MnO_3 at the Γ point are the equations provided by Sato and Tian *et al.* [19,24]. There are four gaps called Δ_{11}, Δ_{12}, Δ_2, Δ_3. In the case of $J_1^c - J_2^c = 0$, these Δ_{11} and Δ_{12} merge into Δ_1, while Δ_2 and Δ_3 becomes $\Delta_2 \sim \Delta_3$, which we denote Δ_2. Here, $\Delta_1 \approx 2S\sqrt{-D_2\lambda_1}$ with $\lambda_1 = D_1 + \frac{3}{2}J_1 + 3J_2$ and $\Delta_2 \approx S\sqrt{2(D_1\lambda_2 + D_2\lambda_3 - 2D_1J_1^c)}$, $\Delta_3 \approx S\sqrt{2(D_1\lambda_2 + D_2\lambda_3 + 3D_2J_2^c)}$ with $\lambda_2 = \frac{3}{2}J_1 + 3J_2$ and $\lambda_3 = 2D_1 + \frac{3}{2}J_1 + 3J_2$. The main factor that determines the size of the gap of the $Lu_{0.47}Sc_{0.53}FeO_3$ is $S\sqrt{\frac{3}{2}J_1 + 3J_2}$. Assuming that J_1 and J_2 remain constant with increasing temperature, the gap closes and disappears at T_N because of the change of the S value. The values of Δ_1 and Δ_2 in *h*-*R*FeO_3 exceed those in *h*-*R*MnO_3 due to the greater magnitude of $S\sqrt{\frac{3}{2}J_1 + 3J_2}$.

TABLE IV. The determined interplanar exchange parameters and magnetic structures of *h*-*R*MnO_3.

2D-TLHAFs	$J_1^c - J_2^c$	Magnetic structure	
$YMnO_3$	0.014(2)	Γ_3	[19]
$YMnO_3$	0.050(5)	Γ_3	[6]
$LuMnO_3$	–0.019(2)	Γ_4	[23]
$Lu_{0.3}Y_{0.7}MnO_3$	–0.012(1)	$C_3\Gamma_3 + C_4\Gamma_4$	This work
$Lu_{0.3}Y_{0.7}MnO_3$	–0.0012(4)	Γ_4	[24]
$YbMnO_3$	–0.012(2)	Γ_4	[6]
$HoMnO_3$	–0.0038(5)	Γ_4	[6]
$HoMnO_3$	0.0018(5)	Γ_1	[6]
$Lu_{0.6}Sc_{0.4}FeO_3$	–	Γ_1	[29]
$Lu_{0.47}Sc_{0.53}FeO_3$	–	$C_1\Gamma_1 + C_2\Gamma_2$	This work

H. Discussion

The magnetic structure and dynamics of 2D triangular Heisenberg antiferromagnets *h*-(Lu,Y)MnO_3 and *h*-(Lu,Sc)FeO_3 have been investigated. These two 2D-TLHAF crystallized with the same symmetry $P6_3cm$. Lu, Y, and Sc are nonmagnetic, while $S = 2$ in Mn^{3+} and $S = \frac{5}{2}$

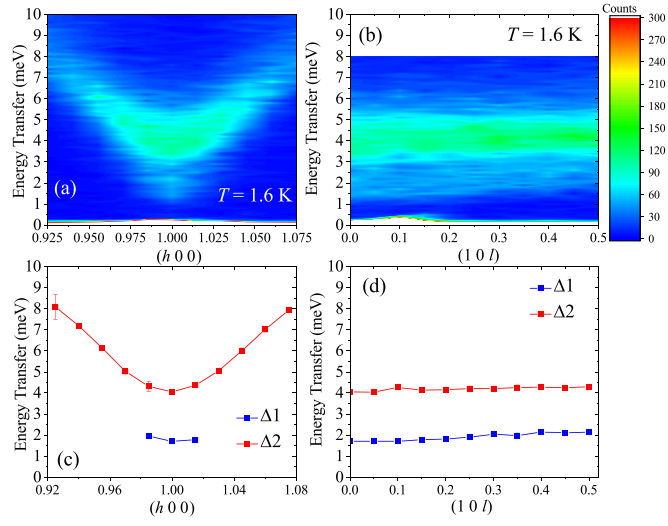

FIG. 8. Spin-wave dispersion of the single-crystal sample of $Lu_{0.47}Sc_{0.53}FeO_3$ observed at $T = 1.5$ K.

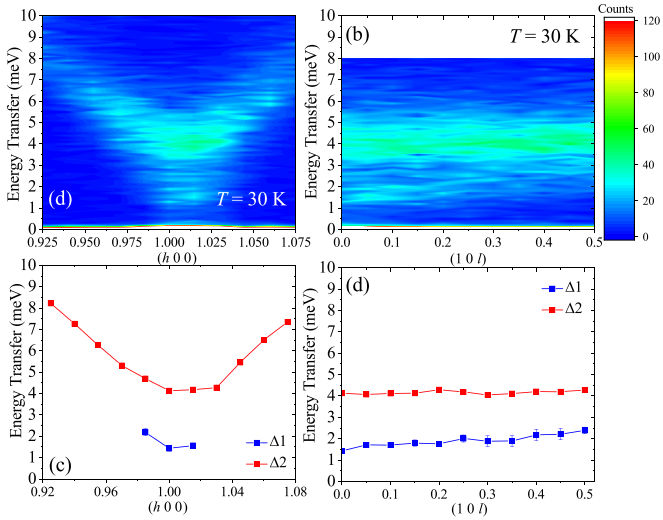

FIG. 9. Spin-wave dispersion of the single-crystal sample of $Lu_{0.47}Sc_{0.53}FeO_3$ observed at $T = 30$ K.

in Fe^{3+}. Unlike previous studies of this system, two irreducible representations were used to solve the magnetic structure of (Lu,Y)MnO_3 and (Lu,Sc)FeO_3. By combining neutron diffraction, polarized neutron diffraction, and inelastic neutron-scattering techniques, we are able to determine the exchange parameters of $Lu_{0.3}Y_{0.7}MnO_3$ with the magnetic structures of these two irreducible representations by using linear spin-wave theory. It should be noted that the neutron-scattering techniques cannot distinguish between the phase coexistence of two single phases with two irreducible representations and one magnetic structure described by two irreducible representations in such a complex magnetic structure.

The utilization of inelastic light-scattering techniques [45] revealed the presence of angularly quantized spin rotations in hexagonal $LuMnO_3$. These 60-, 120-, and 180-degree domains in the plane were viewed as a flat bubble in the sea of the ground state. The work claimed that these angulary quantized spin excitations may lead to high-density information storage of spin devices. The high degree of control for these spin excitations is more easily achieved for isolated Mn or Fe planes. As shown in these spin-wave dispersions from $Lu_{0.3}Y_{0.7}MnO_3$ and $Lu_{0.47}Sc_{0.53}FeO_3$, *h*-*R*FeO_3 could be more suitable for controlling such spin excitations.

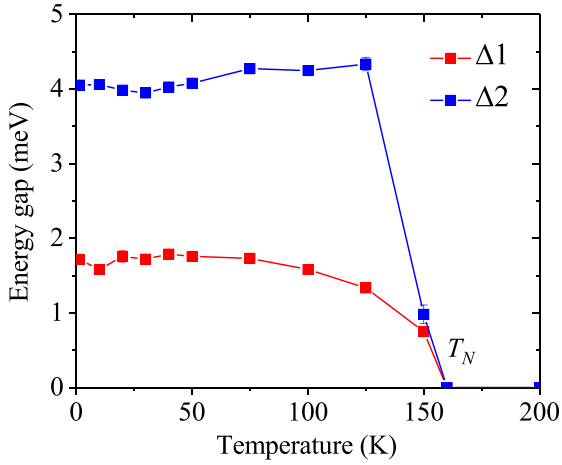

FIG. 10. The temperature dependence of the gaps Δ_1 and Δ_2 of the $Lu_{0.47}Sc_{0.53}FeO_3$.

The question of the existence of two irreducible representations for this system still remains. The result contradicts the statement by Landau and colleagues, that "Every second-order phase transition must occur according to a single irreducible representation," based on the discussion of symmetry in phase transitions [46]. However, as shown in elastic neutron scattering, polarized neutron scattering, and magnetization, these two irreducible representations Γ_1 and Γ_2 are necessary to describe the magnetic structure of *h*-*R*FeO_3, which has not been discussed in the context of magnetic structural analysis and spin reorientations of the *h*-*R*MnO_3 and *h*-*R*FeO_3 systems. Or, if we persist with Landau theory, the combination of (Γ_1 and Γ_2) or (Γ_3 and Γ_4) to describe the magnetic structure implies that the actual crystal symmetry could be $P6_3$, which is a subgroup of $P6_3cm$. We also note that the inhomogeneity of these samples is not detected by the experiments we reported here.

If it is possible to use two irreducible representations to solve the magnetic structures of *h*-*R*MnO_3 and *h*-*R*FeO_3, the spin reorientation behavior of the magnetic structure of 2D-TLHAF reported so far would not be as drastic as claimed. The main reason for the claim that spin reorientation occurs in a 2D-TLHAF system is because we have a clear observation that either Γ_1 and Γ_3 can contribute to the magnetic Bragg peak (100) where there is no nuclear contribution to the Bragg peak, while either Γ_2 and Γ_4 do not contribute to the magnetic Bragg peak (100). However, these (Lu,Y)MnO_3 and (Lu,Sc)FeO_3 suggest that two irreducible representations can be used to describe the magnetic structures, and so-called spin reorientation is not necessary.

No drastic changes in other physical properties, such as specific heat, have been reported. There is a modification of the magnetic structure by adjusting the coefficients of two irreducible magnetic structures. These changes may be better referred to as spin reconfiguration, spin reconciliations, spin adjustment, or just spin rotations. It is possible that the magnetic structure moves while cooling by adjusting these two coefficients of two irreducible representations [37]. Adjustment should occur because of competition between exchange parameters, anisotropic parameters, and Dzyaloshinskii-Moriya (DM) exchange interactions. It is possible to see the interaction of DM-type exchange for *h*-*R*FeO_3 where the weak ferromagnetism is present, but not in *h*-*R*MnO_3.

The source of multiferroicity of this 2D-TLHAF system also needs to be discussed. The *R*-MnO_3 structures have been reported to be type-I multiferroics. In this type of multiferroic, magnetism and ferroelectricity exist independently. To connect magnetism and ferroics, we should have magnetelectric coupling or magnetoelastic coupling. If the magnetic structure consists of Γ_3 or Γ_4, these magnetic structures cannot directly cause ferroelectricity, as shown in Table II [39], and consequently there could be magnetoelastic coupling. As shown in a number of works initiated by Lee *et al.* [17], multiferroicity has until now been considered to be achieved through magnetoelastic coupling. However, Γ_1 or Γ_2 can have

magnetoelectric coupling. So even if the magnetic structures look similar, there can be a different source of multiferroicity. In the case of h-$Lu_{0.6}Sc_{0.4}FeO_3$, Leiner [29] reported electric polarization hysteresis loops and compensated current density under applied electric field along the c axis for the sample on which they performed the neutron-inelastic scattering experiment. Among the four one-dimensional irreducible representations (Γ_{1-4}), only Γ_2 is allowed to have a ferromagnetic moment. The ferromagnetic correlations observed by magnetization and polarized neutron scattering should have been attributed to the magnetic structure Γ_2. In addition to that, as shown in Table 2, magnetoelectric coupling is possible through P_zM_z with the Γ_2 phase. The ferroelectricity and ferromagnetic moment along the c axis are consistent with the coupling. If that is the case, the multiferroicity could be easier to control if the magnetic structure is a source of ferroelectricity.

Regarding the spin dynamics of h-(Lu,Y)MnO_3 and h-(Lu,Sc)FeO_3, we showed that interplanar interactions exist for $Lu_{0.3}Y_{0.7}MnO_3$ but do not for $Lu_{0.47}Sc_{0.53}FeO_3$. A clear dispersion is observed in $Lu_{0.3}Y_{0.7}MnO_3$, while this is absent for $Lu_{0.47}Sc_{0.53}FeO_3$. In the case of $R$$MnO_3$, interplanar interactions and the sign of $J_1^c - J_2^c$ are key parameters in the 2D-TLHAF system, regardless of whether spin reorientation of the system occurs or not. In terms of crystal structure symmetry, these two compounds are the same. However, the intraplanar interactions J_1 and J_2 are greater in h-(Lu, Sc)FeO_3 ($J \sim 4.0$ meV) than in h-(Lu, Y)MnO_3 ($J \sim 2.5$ meV). This would lead to weaker interplanar interactions compared to the intraplanar interactions. If interplanar interactions still exist in $Lu_{0.47}Sc_{0.53}FeO_3$, then the dispersive mode should be captured by these instrument energy resolutions.

Interestingly, Disseler *et al.* [7] considered the systematic behavior of T_N versus the relationship between the lattice parameter c/a of h-$R$$FeO_3$ and h-$R$$MnO_3$. They reported that T_N increases with increasing c/a, oxygen hexahedra become elongated along the c axis, and the distance between the apical oxygen atoms increases when these oxygens do not participate in primary exchange interactions. With these two factors, stronger intraplanar interactions and elongation of the hexahedra lead to the idea that these intraplanar interactions should play a more important role for spin reorientations. Therefore, the more isolated triangular plane could host spin reorientation in this $R$$FeO_3$ system, which so far shows the spin reorientation of all the h-$R$$FeO_3$ showing spin reorientation.

In the case of h-$R$$MnO_3$, so far there is no evidence of correlation between the ratio of the lattice parameters and spin reorientation. Therefore, the primary effect of the spin reorientation of h-$R$$MnO_3$ should be interactions between layers, while the cause of spin reorientation of h-$R$$FeO_3$ could be different. Among h-$R$$MnO_3$ and h-$R$$FeO_3$, it could be argued that the interaction between R-M could exist. In the case of orthochromites $R$$CrO_3$ and orthoferrites $R$$FeO_3$, no spin reorientation has been reported where R are nonmagnetic atoms [9], while some of them show spin reorientations where R are magnetic atoms. Therefore, the interaction R^{3+}-(Mn^{3+} or Fe^{3+}) could be another parameter to investigate further.

In our study of the spin behavior of $Lu_{0.3}Y_{0.7}MnO_3$, the linear spin-wave model effectively describes the excitations. However, incorporating a magnetoelastic model for fitting is beyond the scope of our current research. By including the parameter J_3 in the linear spin-wave model, we have achieved a more accurate representation of the observed spin dynamics. The relationship between J_1 and J_2 deviates significantly from what was predicted by the DFT calculations. Until now, no magnetoelastic excitations in $Lu_{0.6}Sc_{0.4}FeO_3$ have been reported [29]. Therefore, the multiferroic properties of $Lu_{0.6}Sc_{0.4}FeO_3$ do not originate from magnetoelastic coupling, providing further evidence that the origin of multiferroicity in h-$R$$FeO_3$ may differ from that in h-$R$$MnO_3$ systems.

II. SUMMARY

This paper presents an investigation of the magnetic structure and dynamics of 2D triangular Heisenberg antiferromagnets (TLHAFs), with a particular focus on the h-$R$$MnO_3$ and h-$R$$FeO_3$ systems. The study elucidates the origins of the spin orientation phenomena observed in these materials, which are of significant interest because of their complex magnetic interactions and potential multiferroic properties.

The results demonstrate that the magnetic structures of h-$Lu_{0.47}Sc_{0.53}FeO_3$ can be described by a two-dimensional irreducible representation of Γ_6 ($P6_3$), expressed as a linear combination of Γ_1 ($P6_3cm$) and Γ_2 ($P6_3c'm'$). In contrast, the structure of h-$Lu_{0.3}Y_{0.7}MnO_3$ is represented by Γ_5 ($P6_3$), a linear combination of Γ_3 ($P6'_3cm'$) and Γ_4 ($P6'_3cm'$). Based on the precisely determined the magnetic structures, exchange interactions and spin waves of 2D-TLHAF were then investigated. The study also provides evidence of interplanar interactions in h-$Lu_{0.3}Y_{0.7}MnO_3$, which are absent in h-$Lu_{0.47}Sc_{0.53}FeO_3$. Even though these two h-$Lu_{0.3}Y_{0.7}MnO_3$ and h-$Lu_{0.47}Sc_{0.53}FeO_3$ are similar in terms of crystal and magnetic structures, the source of multiferroicity and the origin of spin reorientation could be different.

ACKNOWLEDGMENTS

Financial support for the Sika neutron-scattering instrument comes from the Ministry of Science and Technology, Taiwan (Grant No. MOST 109-2739-M-213-001), and is gratefully acknowledged. S.Y. is financially supported by the National Science and Technology Council of Taiwan, with Grants No. 110-2112-M-213-013, No. 111-2112-M-213-023, No. 112-2112-M-213-019, and No. 113-2112-M-213-011. The work at NJIT was supported by NSF CAREER under Grant No. 2236543. The experiments were performed under the ANSTO user program. The proposal number is Sika (P9906). J-PARC neutron-scattering experiments were performed in BL-12, HRC under these proposals (Proposals No. 2022A0092 and No. 2022B0192)

[1] J. I. Pérez-Landazábal, C. Gómez-Polo, V. Recarte, S. Larumbe, V. Sánchez-Alarcos, M. Fernandes Silva, E. A Gómez Pineda, A. A. Winkler Hechenleitner, M. K. Lima, and J. A. Rodriguez-Velamazán, Morin transition in hematite nanoparticles analyzed by neutron diffraction, J. Phys.: Conf. Ser. **663**, 012003 (2015).

[2] C. H. Rhee, J. T. Lim, C. S. Kim, and S. B. Kim, Neutron diffraction and magnetic properties of $Ba_2Co_2Fe_{12}O_{22}$: Co_2Y, J. Korean Phys. Soc. **62**, 1919 (2013).

[3] M. Hirano, T. Okuda, T. Tsushima, S. Umemura, K. Kohn, and S. Nakamura, Spin configurations and spin reorientations in pure and impurity doped Fe_3BO_6, Solid State Commun. **15**, 1129 (1974).

[4] T. Kozawa, M. Fujihala, T. Uchihara, S. Mitsuda, S. Yano, H. Tamatsukuri, K. Munakata, and A. Nakao, Atomic reconstruction induced by uniaxial stress in MnP, Sci. Rep. **13**, 13750 (2023).

[5] I. Radelytskyi, P. Aleshkevych, D. J. Gawryluk, M. Berkowski, T. Zajarniuk, A. Szewczyk, M. Gutowska, L. Hawelek, P. Wlodarczyk, J. Fink-Finowicki, R. Minikayev, R. Diduszko, Y. Konopelnyk, M. Kozıowski, R. Puzńiak, and H. Szymczak, Structural, magnetic, and magnetocaloric properties of Fe_7Se_8 single crystals, J. Appl. Phys. **124**, 143902 (2018).

[6] X. Fabrèges, S. Petit, I. Mirebeau, S. Pailhès, L. Pinsard, A. Forget, M. T. Fernandez-Diaz, and F. Porcher, Spin-lattice coupling, frustration and magnetic order in multiferroic $R\mathrm{MnO_3}$, Phys. Rev. Lett. **103**, 067204 (2009).

[7] S. M. Disseler, X. Luo, B. Gao, Y. S. Oh, R. Hu, Y. Wang, D. Quintana, A. Zhang, Q. Huang, J. Lau, R. Paul, J. W. Lynn, S.-W. Cheong, and W. Ratcliff, Multiferroicity in doped hexagonal $LuFeO_3$, Phys. Rev. B **92**, 054435 (2015).

[8] Y. S. Tang, S. M. Wang, L. Lin, V. Ovidiu Garlea, Tao Zou, S. H. Zheng, H.-M. Zhang, J. T. Zhou, Z. L. Luo, Z. B. Yan, S. Dong, T. Charlton, and J.-M. Liu, Magnetic structure and multiferroicity of Sc-substituted hexagonal $YbFeO_3$, Phys. Rev. B **103**, 174102 (2021).

[9] T. Yamaguchi, Theory of spin reorientation in rare-earth orthochromites and orthoferrites, J. Phys. Chem. Solids **35**, 479 (1974).

[10] J. Oh, M. D. Le, H.-H. Nahm, H. Sim, J. Jeong, T. G. Perring, H. Woo, K. Nakajima, S. Ohira-Kawamura, Z. Yamani, Y. Yoshida, H. Eisaki, S.-W. Cheong, A. L. Chernyshev, and J.-G. Park, Spontaneous decays of magneto-elastic excitations in non-collinear antiferromagnet (Y, Lu)MnO_3, Nat. Commun. **7**, 13146 (2016).

[11] S. Tóth, B. Wehinger, K. Rolfs, T. Birol, U. Stuhr, H. Takatsu, K. Kimura, T. Kimura, H. M. Rønnow, and C. Rüegg, Electromagnon dispersion probed by inelastic X-ray scattering in $LiCrO_2$, Nat. Commun. **7**, 13547 (2016).

[12] K. Kimura, T. Otani, H. Nakamura, Y. Wakabayashi, and T. Kimura, Lattice distortion coupled with magnetic ordering in a triangular lattice antiferromagnet $CuCrO_2$, J. Phys. Soc. Jpn. **78**, 113710 (2009).

[13] J. Oh, M. D. Le, J. Jeong, J. H. Lee, H. Woo, W.-Y. Song, T. G. Perring, W. J. L. Buyers, S.-W. Cheong, and J.-G. Park, Magnon breakdown in a two dimensional triangular lattice Heisenberg antiferromagnet of multiferroic $LuMnO_3$, Phys. Rev. Lett. **111**, 257202 (2013).

[14] A. Muñoz, J. A. Alonso, M. J. Martínez-Lope, M. T. Casáis, J. L. Martínez, and M. T. Fernández-Díaz, Evolution of the magnetic structure of hexagonal $HoMnO_3$ from neutron powder diffraction data, Chem. Mater. **13**, 1497 (2001).

[15] H. Sim, J. Oh, J. Jeong, M. D. Le and J. G. Park, Hexagonal $RMnO_3$: A model system for two-dimensional triangular lattice antiferromagnets, Acta Crystallogr. B **72**, 3 (2016).

[16] P. J. Brown and T. Chatterji, Neutron diffraction and polarimetric study of the magnetic and crystal structures of $HoMnO_3$ and $YMnO_3$, J. Phys.: Condens. Matter **18**, 10085 (2006).

[17] S. Lee, A. Pirogov, M. Kang, K.-H. Jang, M. Yonemura, T. Kamiyama, S.-W. Cheong, F. Gozzo, N. Shin, H. Kimura, Y. Noda and J.-G. Park, Giant magneto-elastic coupling in multiferroic hexagonal manganites, Nature (London) **451**, 805 (2008).

[18] M. Bieringer and J. E. Greedan, Magnetic structure and spin reorientation transition in $ScMnO_3$, J. Solid State Chem. **143**, 132 (1999).

[19] T. J. Sato, S.-H. Lee, T. Katsufuji, M. Masaki, S. Park, J. R. D. Copley, and H. Takagi, Unconventional spin fluctuations in the hexagonal antiferromagnet $YMnO_3$, Phys. Rev. B **68**, 014432 (2003).

[20] T. Chartterji, Neutron scattering investigations of multiferroic $YMnO_3$, Pramana J. Phys. **71**, 847 (2008).

[21] S. Petit, F. Moussa, M. Hennion, S. Pailhès, L. Pinsard-Gaudart, and A. Ivanov, Spin phonon coupling in hexagonal multiferroic $YMnO_3$, Phys. Rev. Lett. **99**, 266604 (2007).

[22] S. L. Holm, A. Kreisel, T. K. Schäffer, A. Bakke, M. Bertelsen, U. B. Hansen, M. Retuerto, J. Larsen, D. Prabhakaran, P. P. Deen, Z. Yamani, J. O. Birk, U. Stuhr, Ch. Niedermayer, A. L. Fennell, B. M. Andersen, and K. Lefmann, Magnetic ground state and magnon-phonon interaction in multiferroic h-$YMnO_3$, Phys. Rev. B **97**, 134304 (2018).

[23] H. J. Lewtas, A. T. Boothroyd, M. Rotter, D. Prabhakaran, H. Müller, M. D. Le, B. Roessli, J. Gavilano, and P. Bourges, Magnetic excitations in multiferroic $LuMnO_3$ studied by inelastic neutron scattering, Phys. Rev. B **82**, 184420 (2010).

[24] W. Tian, G. Tan, L. Liu, J. Zhang, B. Winn, T. Hong, J. A. Fernandez-Baca, C. Zhang, and P. Dai, Influence of doping on the spin dynamics and magnetoelectric effect in hexagonal $Y_{0.7}Lu_{0.3}MnO_3$, Phys. Rev. B **89**, 144417 (2014).

[25] T. Kim, J. C. Leiner, K. Park, J. Oh, H. Sim, K. Iida, K. Kamazawa, and J.-G. Park, Renormalization of spin excitations in hexagonal $HoMnO_3$ by magnon-phonon coupling, Phys. Rev. B **97**, 201113(R) (2018).

[26] L. Lin, H. M. Zhang, M. F. Liu, S. Shen, S. Zhou, D. Li, X. Wang, Z. B. Yan, Z. D. Zhang, J. Zhao, S. Dong, and J.-M. Liu, Hexagonal phase stabilization and magnetic orders of multiferroic $Lu_{1-x}Sc_xFeO_3$, Phys. Rev. B **93**, 075146 (2016).

[27] J. Yang, C. Duan, J. R. D. Copley, C. M. Brown, and D. Louca, The magnetic transitions and dynamics in the multiferroic $Lu_{0.5}Sc_{0.5}FeO_3$, MRS Adv. **1**, 565 (2016).

[28] A. Masuno, A. Ishimoto, C. Moriyoshi, N. Hayashi, H. Kawaji, Y. Kuroiwa, and H. Inoue, Weak ferromagnetic transition with a dielectric anomaly in hexagonal $Lu_{0.5}Sc_{0.5}FeO_3$, Inorg. Chem. **52**, 11889 (2013).

[29] J. C. Leiner, T. Kim, K. Park, J. Oh, T. G. Perring, H. C. Walker, X. Xu, Y. Wang, S.-W. Cheong, and J.-G. Park, Magnetic excitations in the bulk multiferroic two-dimensional triangular lattice antiferromagnet (Lu, Sc)FeO_3, Phys. Rev. B **98**, 134412 (2018).

[30] M. Avdeev and J. R. Hester, ECHIDNA: A decade of high-resolution neutron powder diffraction at OPAL, J. Appl. Crystallogr. **51**, 1597 (2018).

[31] C.-M. Wu, G. Deng, J. S. Gardner, P. Vorderwisch, W.-H. Li, S. Yano, J.-C. Peng, and E. Imamovic, SIKA–The multiplexing cold-neutron triple-axis spectrometer at ANSTO, JINST **11**, P10009 (2016).

[32] S. Yano, G. N. Iles, J.-Ch. Peng, and Ch.-M. Wu, Current status of the Taiwanese cold triple axis spectrometer, SIKA, at ANSTO, J. Surf. Investig. **14**, S207 (2020).

[33] S. Itoh, T. Yokoo, S. Satoh, S. Yano, D. Kawana, J. Suzuki, and T. J. Sato, High resolution chopper spectrometer (HRC) at J-PARC, Nucl. Instrum. Methods Phys. Res., Sect. A **631**, 90 (2011).

[34] S. Itoh, T. Yokoo, T. Masuda, S. Asai, H. Saito, D. Kawana, R. Sugiura, T. Asami, and Y. Ihata, Progress in high resolution chopper spectrometer HRC by improving collimator and Fermi chopper, Phys. B: Condens. Matter **568**, 76 (2019).

[35] W. Tung (Hal) Lee and T. D'Adam, Polarised neutron scattering capability at ANSTO, Neutron News **27**, 35 (2016).

[36] A. G. Manning, S. Yano, S. Kim, W. B. Lee, S.-H. Choi, and N. R. de Souza, Identifying the spin-incoherent contribution to quasielastic neutron scattering with a cold triple-axis spectrometer, Quantum Beam Sci. **7**, 35 (2023).

[37] S. Yano, C.-W. Wang, J. S. Gardner, W.-T. Chen, K. Iida, R. A. Mole, and D. Louca, Weak trimerization in the frustrated two-dimensional triangular Heisenberg antiferromagnet $Lu_yY_{1-y}MnO_3$, Phys. Rev. B **107**, 214407 (2023).

[38] S. Janas, J. Lass, A.-E. Ţuţueanu, M. L. Haubro, C. Niedermayer, U. Stuhr, G. Xu, D. Prabhakaran, P. P. Deen, S. Holm-Dahlin, and K. Lefmann, Classical spin liquid or extended critical range in h-$YMnO_3$? Phys. Rev. Lett. **126**, 107203 (2021).

[39] C. J. Howard, B. J. Campbell, H. T. Stokes, M. A. Carpenter, and R. I. Thomson, Crystal and magnetic structures of hexagonal $YMnO_3$, Acta Cryst. **B69**, 534 (2013).

[40] M. Ramakrishnan, Y. Joly, Q. N. Meier, M. Fechner, M. Porer, S. Parchenko, Y. W. Windsor, E. M. Bothschafter, F. Lichtenberg, and U. Staub, Antiferromagnetic spin canting and magnetoelectric multipoles in h-$YMnO_3$, Phys. Rev. Res. **5**, 013203 (2023).

[41] S. W. Lovesey, Axial and polar magnetism in hexagonal $YMnO_3$, Phys. Rev. B **108**, 104412 (2023).

[42] I. V. Solovyev, M. V. Valentyuk, and V. V. Mazurenko, Magnetic structure of hexagonal $YMnO_3$ and $LuMnO_3$ from a microscopic point of view, Phys. Rev. B **86**, 054407 (2012).

[43] K. Park, J. Oh, K. H. Lee, J. C. Leiner, H. Sim, H.-H. Nahm, T. Kim, J. Jeong, D. Ishikawa, A. Q. R. Baron, and J.-G. Park, Magnetoelastic excitations in multiferroic hexagonal $YMnO_3$ studied by inelastic x-ray scattering, Phys. Rev. B **102**, 085110 (2020).

[44] A. L. Chernyshev and W. Brenig, Thermal conductivity in large-J two-dimensional antiferromagnets: Role of phonon scattering, Phys. Rev. B **92**, 054409 (2015).

[45] S. Kim, J. Nam, X. Xu, S. W. Cheong, and In-SangYang, Angularly quantized spin rotations in hexagonal $LuMnO_3$, Sci. Rep. **12**, 2424 (2022).

[46] Z. L. Davies, Application of representation theory to magnetic and structural phase transitions, Ph.D. thesis, University College London, 2009.